HENRY

Hydraulic Engineering Repository

Ein Service der Bundesanstalt für Wasserbau

Conference Paper, Published Version

Radice, Alessio; Ballio, Francesco; Armenio, V.; Franzetti, Silvio

Scour development and sediment motion at rectangular and trapezoidal abutments

Verfügbar unter/Available at: https://hdl.handle.net/20.500.11970/100065

Vorgeschlagene Zitierweise/Suggested citation:
Radice, Alessio; Ballio, Francesco; Armenio, V.; Franzetti, Silvio (2006): Scour development and sediment motion at rectangular and trapezoidal abutments. In: Verheij, H.J.; Hoffmans, Gijs J. (Hg.): Proceedings 3rd International Conference on Scour and Erosion (ICSE-3). November 1-3, 2006, Amsterdam, The Netherlands. Gouda (NL): CURNET. S. 547-555.

Scour development and sediment motion at rectangular and trapezoidal abutments

A. Radice[*], F. Ballio[*], V. Armenio[**] and S. Franzetti[*]

[*] Politecnico di Milano, Dept. I.I.A.R., Milan, Italy
[**] Università degli Studi di Trieste, Dept. Of Civ. Eng., Trieste, Italy

We present results of abutment scour experiments in a pressurized rectangular duct. Two obstacles of different shape were tested: a vertical plate and a 45° trapezoidal abutment. During the experiments, scour depths were measured all around the abutments; both tests were repeated several times to verify repeatability of the erosion trends. Sediment motion was filmed from the top via a digital CCD; concentration and velocity of the moving grains were measured by image processing. The measured scour trend at the vertical plate is not different from those measured in previous experiments with a free surface, showing that the pressurized flow does not significantly influence the erosion development and the scour hole shape. Maximum scour depths at the trapezoidal abutment were almost 25% less than those at the vertical plate; the shape effect is consistent with the results from literature free surface experiments. For both the abutment types, sediment activity is intense in the first part of the process, it then becoming weaker as time proceeds. Measurements of the instantaneous values of sediment concentration and velocity show that variability in space and time of the solid discharge magnitude and direction increases in the meantime; unsteadiness of grain kinematics indicates similar features of the scour inducing flow field. The obstacle shape influences the intensity of sediment motion: experimental results show that the absence of a blunt obstruction to the mean flow in case of a trapezoidal abutment determines a weaker sediment activity than that for the vertical plate.

I. INTRODUCTION

Local scour at bridge structures has been extensively studied over the past fifty years, mainly by means of laboratory experimentation (see for example [1] and [2]). Such approach allows for individuating the effect of the system control parameters on the erosion trend, without exploring in detail the dynamics of the scour process at a small scale. Thus, little scale phenomenological studies may be a good complement to the large scale ones.

Both experimental and numerical studies of the three dimensional flow field that develops in the proximity of bridge structures can be found in the scientific literature (see for example ref. from [3] to [7]). Visualization of the instantaneous flow field showed the presence of unstable coherent structures of significant dimension in comparison to that of the obstacle. Analysis of the average structure of the flow field highlighted the presence of the horseshoe vortex and of the principal vortex system, that are generally considered the main scouring agents at bridge piers and abutments, respectively.

In this paper we focus on sediment motion around a bridge abutment. Particle entrainment and transport is direct consequence of the action of the scouring flow field; therefore, analyzing the kinematics of the solid phase can considerably support the study of the flow field in investigating the dynamics of the scour process at the particle scale. Some previous works by the Authors (ref. from [8] to [11]) showed that availability of data on the sediment motion can help the interpretation of the process features.

We measured sediment kinematics by filming the scour phenomenon in process and then applying some recent image processing techniques to the acquired movies. We performed the experiments in a closed transparent duct to allow for a clear vision of the process.

We used two obstacles, a vertical plate and a 45° trapezoidal abutment. It is well known that trapezoidal abutments lead to smaller scour depths than vertical ones having the same width (see for example [12]).

We compared the sediment kinematics we obtained for the two abutment shapes, in order to infer similarities in the scouring flow fields for the two cases, as well as discrepancies that could be responsible for the differences in the scour depth trends. Prior to analysis of the sediment motion, we verified that our scour reduction factor was consistent with that given in the literature, in order to check for any possible distortion due to the absence of a free surface.

II. EXPERIMENTAL SETUP

The experimental duct is 5.8 m long, with a rectangular transversal section having width and height equal to 40 and 16 cm, respectively. The whole duct is made of plexiglass to assure complete transparency of the walls. An upstream and a downstream tank complete the experimental installation; the hydraulic head in the duct is imposed by a Bazin weir posed in the outlet tank. Water entrance in the duct is guided by a streamlined inlet to avoid wake effects in the flow.

The test reach of the duct is deeper than the other parts; it was filled with PVC cylinders having median equivalent diameter $d_{50} = 3.6$ mm, a uniformity coefficient very close to 1 and specific gravity $\Delta = (\rho_s - \rho)/\rho = 0.43$, where ρ_s and ρ are the densities of sediments and water, respectively. In the upstream and downstream reaches, the same bed roughness is obtained by gluing the PVC grains to steel sheets posed onto the duct bottom; as a result, the effective duct height is $h = 15.5$ cm.

The abutment model is located at about 3.4 m from the duct inlet; we used two different abutments, being the first

a vertical plate and the second a 45° trapezoidal abutment. Both obstacles were made of transparent PVC. Abutment length was b = 10 cm and b = 8 cm for the rectangular and trapezoidal abutments, respectively (Fig. 1).

Water discharge is measured by a magnetic flowmeter posed on the delivery pipe.

The scour depth d at the abutment nose (see Fig. 1) was continuously measured by a laser distance sensor posed just over the duct ceil. The scour depth at the channel wall was visually measured by a rule on the same wall. During the test, the scouring process was filmed via a black and white CCD capable of 50 fps with a resolution of 576 x 763 pixel. Duration of every movie was equal to 20 s. Profiles of transversal and longitudinal sections of the scour hole were surveyed one or two times during the tests, in order to measure also the scour hole shape.

We performed some experimental runs with the same water discharge (Q = 18.5 l/s), to verify repeatability of the experimental procedure. The selected water discharge corresponded to the incipient motion of the bed particles.

The characteristics of the experimental tests are given in Table 1. Only for experiments 1 to 8 the scour depth was measured via the laser distance sensor; in the remaining experiments (tests 9 and 10) the laser was not used to guarantee a good visibility for the CCD and thus a large focus area. The CCD and the laser were used jointly during the other experiments with a vertical plate (1, 2, 6 and 8), but the visualization area was considerably smaller than that we will present in this work (see [10] and [11]).
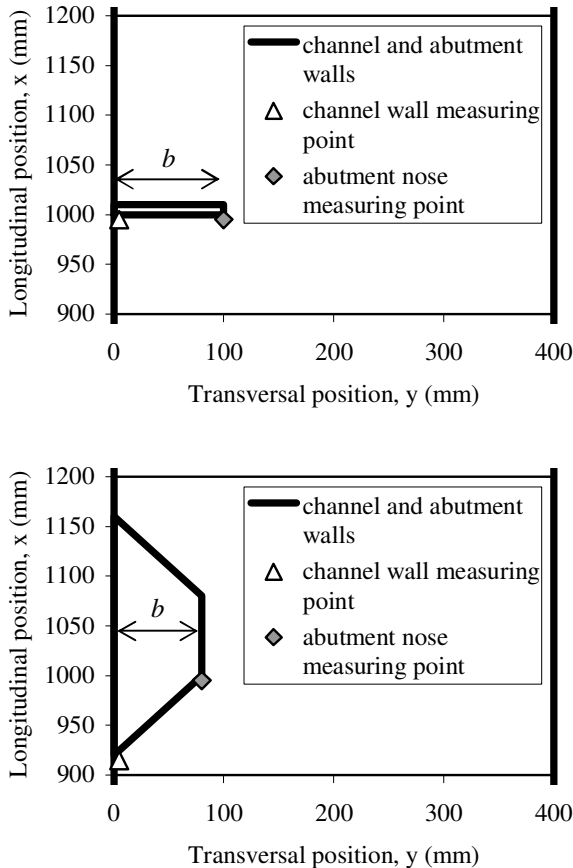

Figure 1. Definition sketch. Vertical wall (up) and 45° wing wall (down) abutments. Water flow is from bottom to top

TABLE I. EXPERIMENTAL TESTS

Test	Abutment
1, 2, 6, 8	Vertical plate
3, 4	Trapezoidal
9	Trapezoidal
10	Vertical plate

III. SCOUR DEVELOPMENT

The temporal development of the scour depth at the vertical plate is shown in Fig. 2. Local erosion trend presents the classical features that are typically observed during experiments with a free surface; scour depth continuously grows with time, but at a decreasing rate. The temporal trend at the abutment nose can be approximated by two straight segments having different slopes in the semi-logarithmic plane; the temporal trend at the channel wall starts later than at the nose, and it is approximated by a straight line of similar slope to that of the first line for the abutment nose. As a consequence, maximum scour depth is initially located at the abutment nose, but later it moves towards the channel wall; intersection between the two scour trends occurs for a time T of about 800 s, corresponding to a dimensionless time $\tau = TU/b \cong 2.4 \cdot 10^3$, where U is water velocity and b is the abutment length.

Fig. 3 presents the temporal trends of the scour depth at the trapezoidal abutment. Also in this case the scour depth continuously grows with time. The rate of the erosion depth in the semi-logarithmic plane is variable till a time $T \cong 3000$ s, corresponding to a dimensionless time $\tau \cong 1.1 \cdot 10^4$; then, the scour trend can be approximated by a straight line. The scour depth at the channel wall follows a similar evolution, even if the activation is later and the rate is larger than that at the abutment nose. Differently from the vertical wall abutment, no intersection between the two scour trends was observed for the final dimensionless time, $\tau \cong 9 \cdot 10^5$. Thus, the abutment shape influences the location of the maximum scour depth around the obstacle.

The dimensionless evolution of the maximum scour depth is presented in Fig. 4 for all the experimental tests where the laser sensor was used. The local scour depth d was normalized via the abutment length b. The superimposition of all the curves shows the good repeatability of the experiments.

The scour depth at the vertical abutment is larger than that at the trapezoidal one. Ref. [12] defined a scour reduction factor K_s depending on the abutment shape, indicating 0.75 as the K_s value for a 45° wing wall abutment. Even if the shape coefficient was defined by [12] with reference to the equilibrium scour depth and not to the temporal trend of the erosion, present results are substantially in agreement with previous findings: for the dimensionless time τ = 10^4, for example, the ratio between the scour depths at the trapezoidal abutment and at the vertical plate is equal to the literature value of K_s.

Data from the surveys of the longitudinal and transversal sections of the scour hole were processed via a kriging interpolator to obtain the contour lines of the hole; these are showed in Fig. 5. The scour hole shape at the vertical wall abutment is consistent to that found for example by [13]: the maximum scour depth is located upstream of the abutment, in the proximity of the channel

wall, with the upstream part of the scour hole being similar to an inverted cone. Upstream of the abutment nose a sort of sediment hill is present, whose existence is highlighted by the irregular shape of the contour line corresponding to $-d/b = -1.8$ for $x \cong 950$ mm, $y \cong 90$ mm. In the downstream part of the hole, two parallel channels develop, that are separated by a sediment ridge. For the trapezoidal abutment, the maximum scour depth is located near the abutment nose; the upstream part of the scour hole is similar to an inverted cone, but in this case the sediment hill upstream of the abutment nose is hardly present. Also the downstream part is significantly different from that at the vertical plate, in that only one sediment channel is present. One possible reason for this feature may be the fact that the flow reattachment to the lateral wall is progressively guided by the streamlined abutment shape in case of the trapezoidal obstacle; this would indicate the larger wake as responsible of the formation of the left sediment channel for the vertical plate. Contour lines of the scour hole are consistent with previous literature findings (see [14] and [15]).

Present results demonstrate that scour experiments in a pressurized duct are similar to those for a free surface stream; thus, our results for sediment motion around the obstacles will be good indicators also for the dynamics of the scour process in free surface experiments.
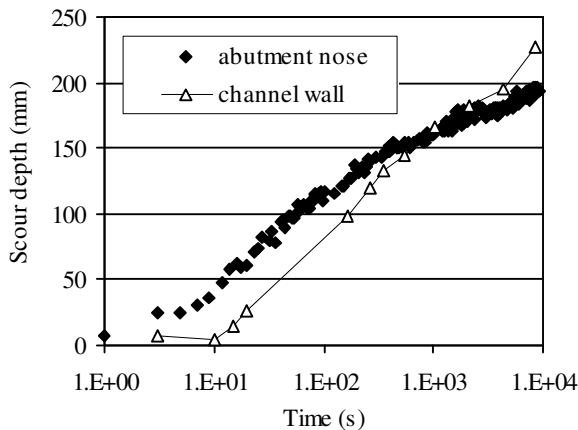
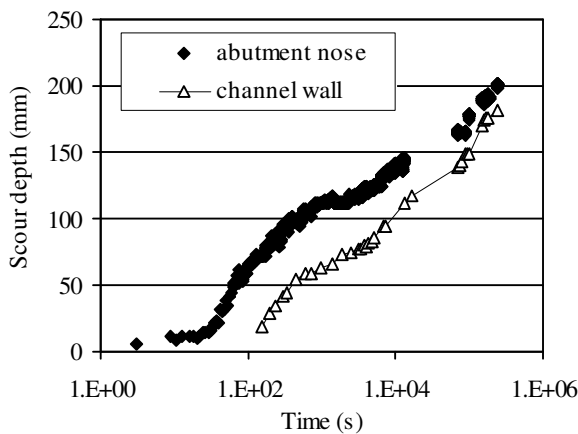Figure 2.   Time development of scour depth at the vertical plate (test 1)

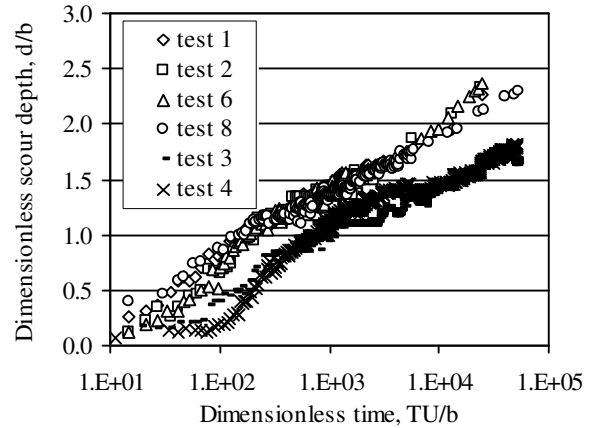Figure 3.   Time development of scour depth at the trapezoidal abutment (test 4)

Figure 4.   Dimensionless time development of maximum scour depth for the experimental tests

IV.   IMAGE PROCESSING

Measurement of concentration and velocity of the moving particles allows for evaluation of the sediment fluxes around the obstacles. In fact, the vector solid discharge per unit width (hereafter simply called solid discharge) can be calculated as $q_s = C \cdot v_s \cdot d_{50}$, where C is the aerial sediment concentration and v_s is sediment velocity.

Sediment concentration (see [8]) was measured via an image difference technique: consecutive frames in a movie were subtracted to highlight the occurred movements; the difference images were then thresholded and filtered to eliminate the noise and to obtain the final image of the displaced particles. After counting the number of displaced particles N, the corresponding sediment concentration could be easily calculated as $C = (N \cdot W_g)/(\Delta x \cdot \Delta y \cdot d_{50})$, where W_g is the volume of a single particle, and Δx and Δy are the dimensions of the measuring cell. Sediment velocity was measured by applying a Particle Image Velocimetry algorithm to a couple of successive difference images (see [9]).

Measures of both grain concentration and velocity require definition of spatial and temporal support scales, that have to satisfy opposite requirements. The spatial measuring scale has to be large enough in comparison to grain dimension, to allow for an eulerian representation of movement; on the contrary, it has to be small enough to allow observing the spatial variability of grain motion. The temporal measuring scale has to be large enough to observe non vanishing grain movements between one instant and the next; on the contrary, a too long temporal scale compromises the measures due to dispersion of the grains. In this work, we used spatial measuring cells whose dimension was 2 cm x 2 cm, while the time sampling interval was the maximum allowed by the CCD, i.e. 0.02 s. Effect of variation of the support scales on the measure are described in [16].
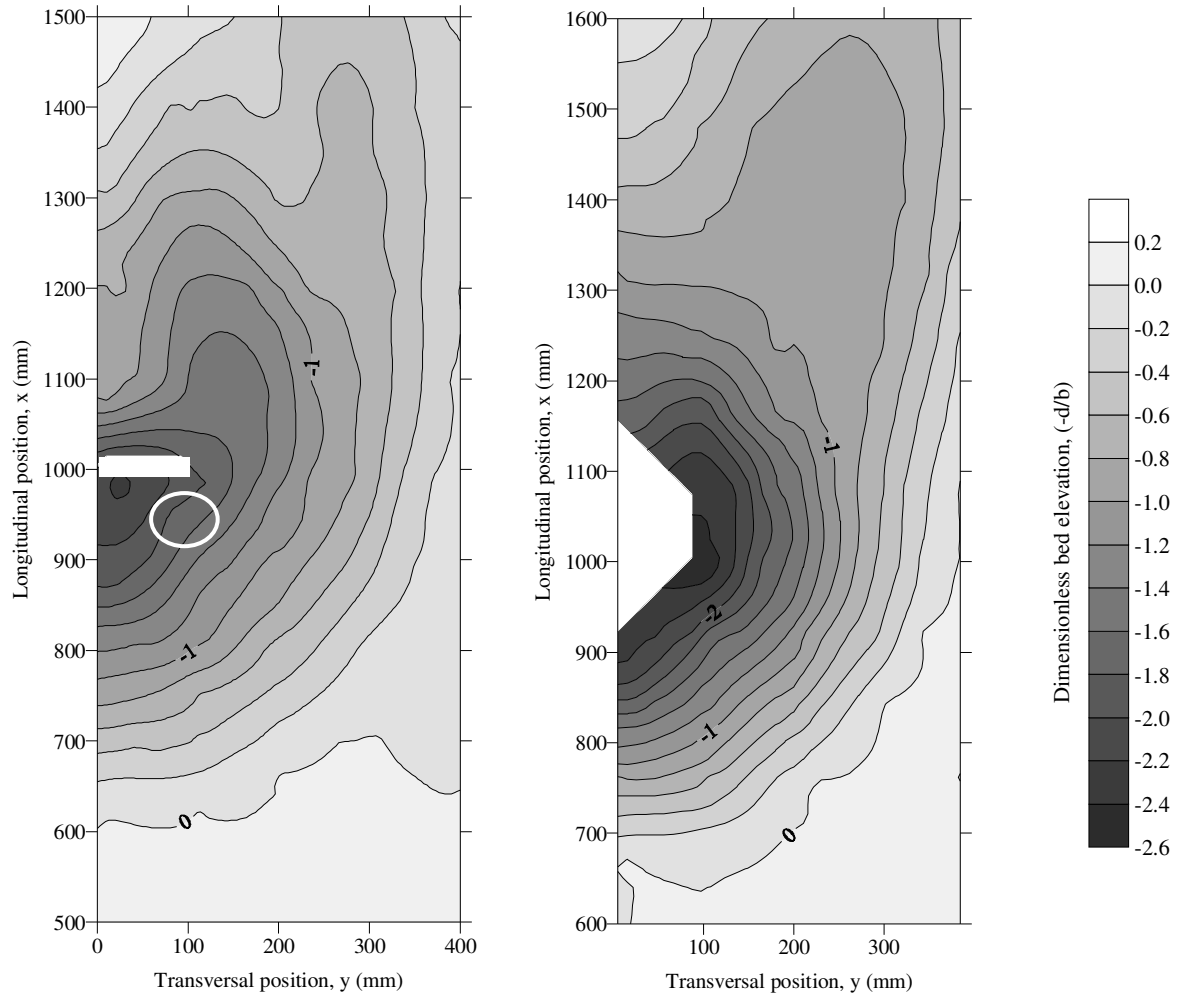
Figure 5. Contour lines of the bed elevation around the vertical plate (left) and the trapezoidal abutment (right), for similar scour levels. For the vertical plate test 1 is considered at time T = 9900 s; for the trapezoidal obstacle one test 4 is considered at time T = 2.4·10⁵ s. Colour scale is proportional to dimensionless bed elevation measured from the original non-scoured bed. Water flow is from bottom to top; the sediment hill upstream of the vertical plate nose is highlighted
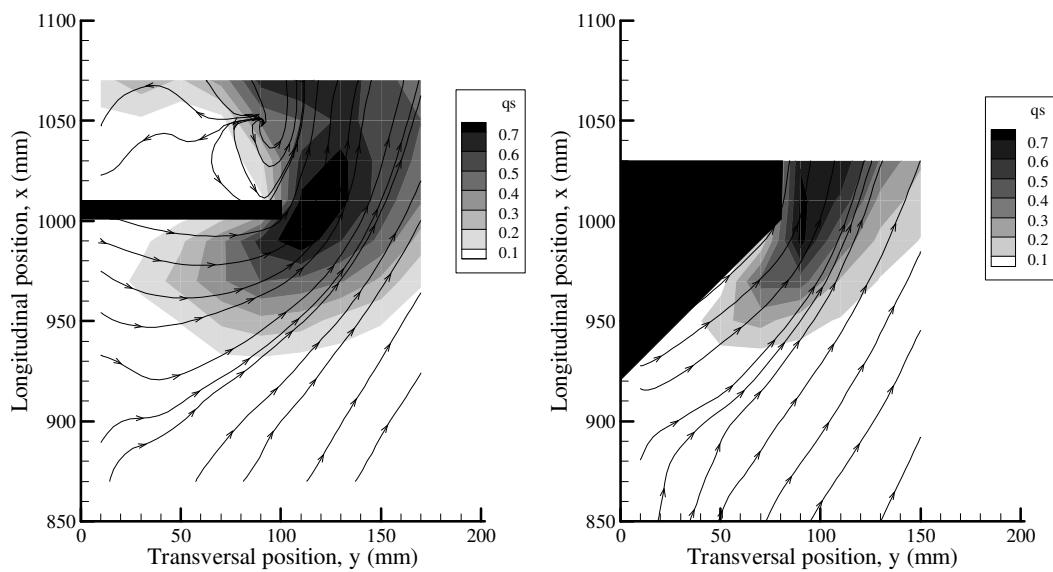

Figure 6. Mean solid discharge fields for the test start (T < 20 s) at the vertical plate (test 10, left) and at the trapezoidal abutment (test 9, right). Colour scales are proportional to the module of average solid discharge (q_s) in cm²/s

Figure 7. Mean solid discharge fields for d/b ≅ 1.20 at the vertical plate (test 10, T = 100 s, left) and at the trapezoidal abutment (test 9, T = 420 s, right). Colour scales are proportional to the module of average solid discharge (q_s) in cm^2/s

Figure 8. Mean solid discharge fields for d/b ≅ 1.40 at the vertical plate (test 10, T = 270 s, left) and at the trapezoidal abutment (test 9, T = 18000 s, right). Colour scales are proportional to the module of average solid discharge (q_s) in cm^2/s
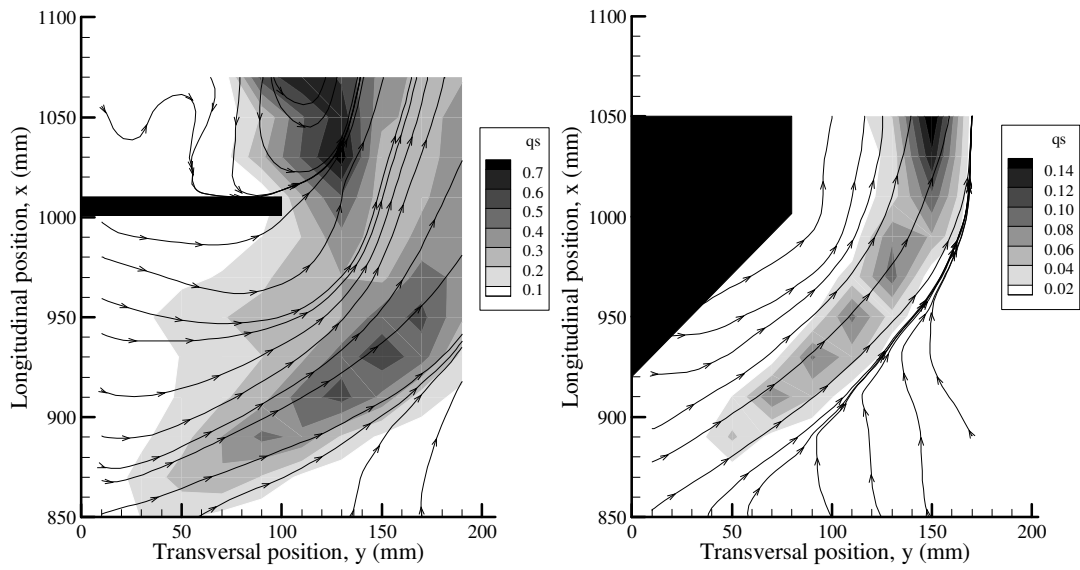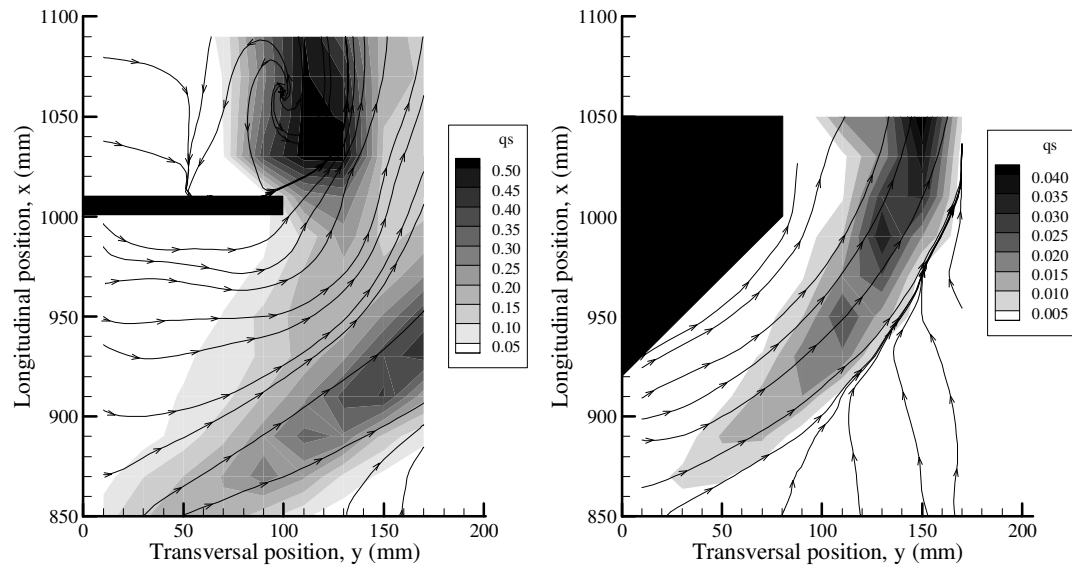
Figure 9.   Mean solid discharge fields for d/b ≅ 1.80 at the vertical plate (test 10, T = 2900 s, left) and at the trapezoidal abutment (test 9, T = 14000 s, right). Colour scales are proportional to the module of average solid discharge (q_s) in cm^2/s

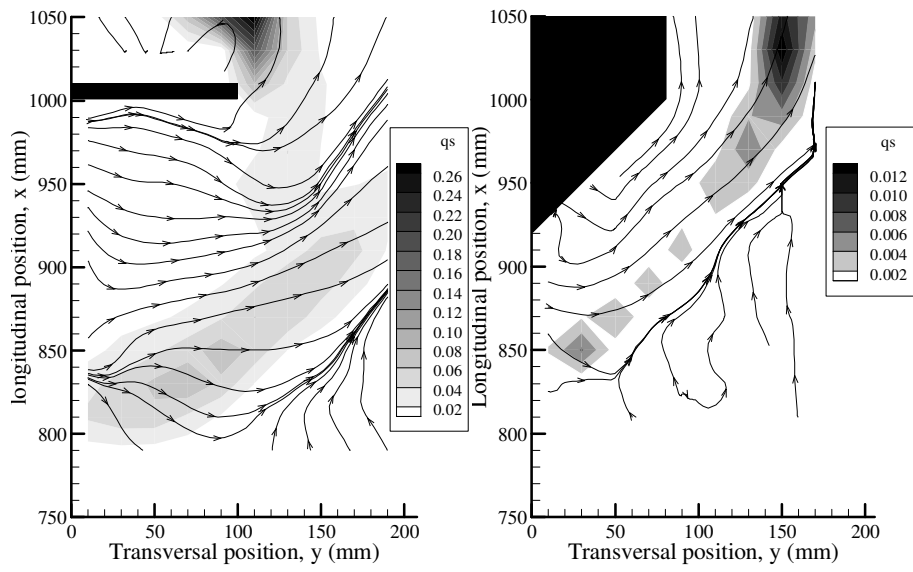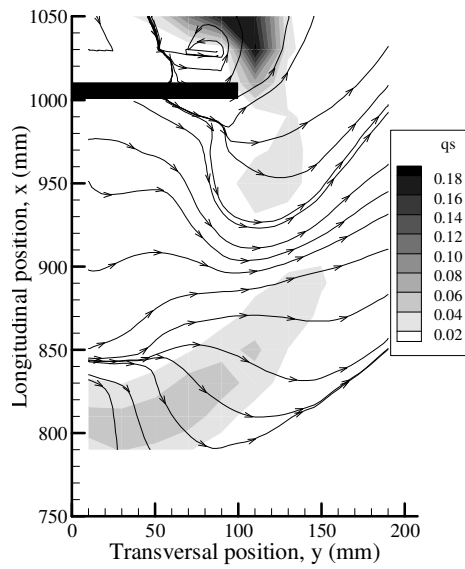Figure 10. Mean solid discharge at the vertical plate (test 10, T = 7500 s). Colour scale is proportional to the module of average solid discharge (q_s) in cm^2/s

Figure 11. Variation coefficient of solid discharge for d/b ≅ 1.20 at the vertical plate (test 10, T = 100 s, left) and at the trapezoidal abutment (test 9, T = 420 s, right). The corresponding solid discharge fields are presented in Fig. 7
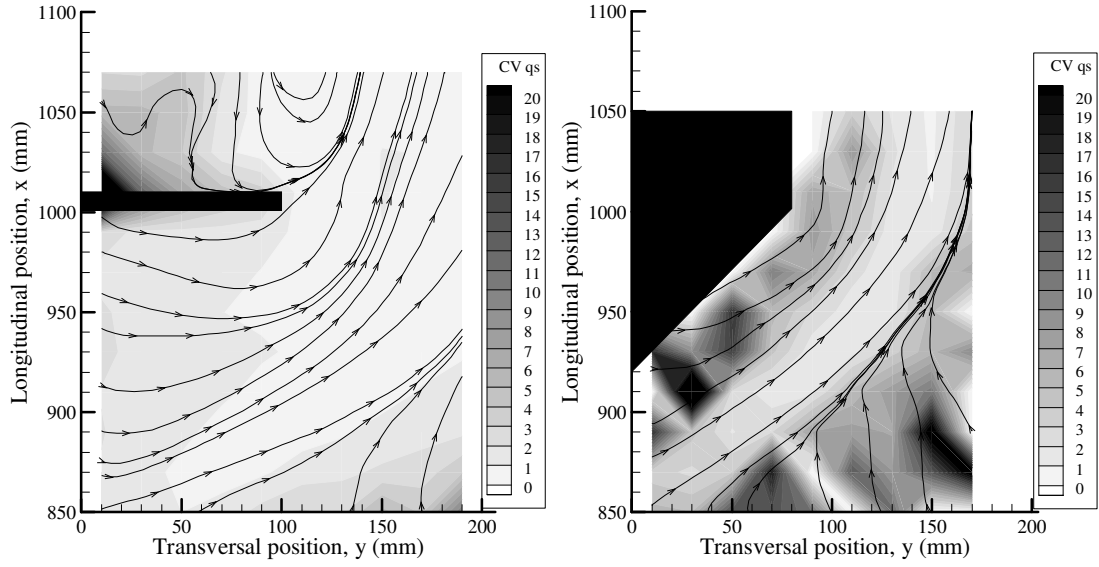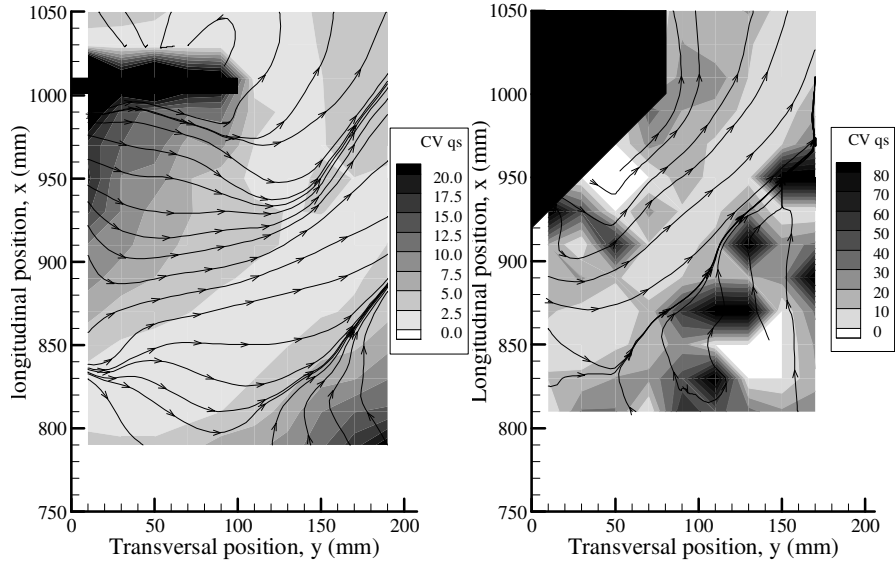

Figure 12. Variation coefficient of solid discharge for d/b ≅ 1.80 at the vertical plate (test 10, T = 2900 s, left) and at the trapezoidal abutment (test 9, T = 14000 s, right). The corresponding solid discharge fields are presented in Fig. 9

V. SEDIMENT MOTION

Analysis of the sediment motion will be made through observation of the spatial distribution of the time average solid discharge. The latter can be computed in two ways:

$$q_{s(1)} = \sqrt{\left(\sum_{i=1}^{n} \frac{q_{sx,i}}{n}\right)^2 + \left(\sum_{i=1}^{n} \frac{q_{sy,i}}{n}\right)^2} \qquad (1);$$

$$q_{s(2)} = \frac{1}{n}\sum_{i=1}^{n} \sqrt{q_{sx,i}^2 + q_{sy,i}^2} \qquad (2).$$

In (1) and (2), q_{sx} and q_{sy} are the components of the solid discharge along the coordinate axes, n is the sample dimension, q_s is the average solid discharge. Evaluating the latter by (1) gives the magnitude obtained by the time average components of the vector solid discharge, while (2) furnishes the time average magnitude of the instantaneous solid discharges. The information one

obtains from the two quantities is different: (1) is related to the resulting structure of the solid discharge field, while (2) is proportional to the average intensity of sediment motion regardless of the direction. Typically the solid discharge evaluated by (1) is smaller than that obtained via (2), since the presence of movements having different directions reduces the average components of the final vector. For a comparison between the spatial distributions of the two quantities see [10]. In the following, spatial distributions of the time average magnitude of solid discharge by (2) will be shown, together with average streamlines obtained via the solid discharge calculated via (1).

Fig. 6 presents the average sediment fluxes around the obstacles for the initial stage of the experiments (time T < 20 s). In this phase the scour rate is maximum, as it is shown in Figs. 2 and 3. Maximum sediment activity is located in the proximity of the abutment nose in both cases, with similar maximum values of the solid discharge. Spatial distribution of the average sediment flux is consistent with previous literature indications on the average shear stress distribution around the obstacles (see for example [17] and [18]), which presents a maximum at the abutment nose due to the flow concentration in the same position. Higher solid discharges span a wider area in the case of the vertical wall abutment, indicating a larger intensity of the flow field, that is reasonably due to the bluntness of the obstacle. The large solid discharges around the abutments are not directly linked to the great erosive power in this phase, since the scour rate is related to the spatial variation of the sediment flux and not to the maximum flux values; yet it is reasonable that larger solid discharge values will result in a larger divergence of the vector flux, and thus in a larger erosion depth.

The average streamlines turn around the obstacles, with increasing solid discharge as the streamlines are travelled; this effect is due to the progressive entrainment of new sediments, that join to those coming from upstream. Sporadic upward direction were measured for both the abutments near the channel lateral wall. Literature visualizations of the scouring flow field around rectangular and trapezoidal abutments in the flat bed condition ([18] and [19]) showed the presence of the principal vortex structure, that would result in diffuse upward sediment movements. Present findings show that the principal vortex is, on average, highly stretched along the mean flow direction, and upward movements are limited to the wall region. For the rectangular abutment the recirculation area downstream of the obstacle was filmed; the wake vortex, whose trace is evident from the observation of the average streamlines, appears to be responsible for high solid fluxes.

As the scour depth increases, the sediment pattern around the obstacles varies. We show the average sediment movement fields at the two obstacles for similar values of the dimensionless scour depth, regardless of the time needed to reach such erosion levels. The effect of the abutment shape on the temporal development of the erosion depth was already shown (Fig. 4); now we intend to investigate the effect of the abutment shape in determining the flow field and thus the sediment pattern on a similar scour hole. Results are presented in Figs. 7 and 8. The average solid discharge decreases at both the obstacles as larger scour levels are achieved, due to the

flow field weakening that is consequent to the increase in the area available for the flow conveyance. Sediment fluxes at the trapezoidal abutment are smaller than those at the vertical plate, owing to the fact that the streamlined obstacle produces a weaker recirculation of the flow. The area where sediment activity is larger spans a sort of circumference around the obstacle nose; it is remarkable to note that near the obstacle walls the solid discharge flux is weak, indicating that the flow field is inhibited by the corner between the abutment face and the bed. Actually shear distributions on a scoured bed around bridge piers present a maximum in a region that is qualitatively consistent to that where we observed the maximum sediment fluxes (see [20]). The large activity region delimits two parts of the scour hole; in the inner one (that closer to the abutment) the sediments are moved by the flow field and conveyed downstream around the obstacle. In the outer one the sediments either slide along the scour hole or are displaced by occasional transport events, with a longitudinal direction; as they arrive at the active zone, they are entrained by the principal movement. The above effect is more evident for the trapezoidal abutment thanks to the small dimension of the inner area, that instead covered nearly all the image for the vertical plate. The average solid discharge increases along the streamlines, as was previously noticed for the initial phase of the erosion process. In this phase the action of the principal vortex is clearer for the vertical plate, where upward movements were measured upstream of the abutment nose. The effect of the wake downstream of the vertical plate is still clearly identifiable.

Figure 9 presents the solid discharge fields for a more developed condition (dimensionless scour depth d/b is equal to 1.80). For the vertical plate, the focus area of the CCD was shifted upstream to capture the upstream part of the scour hole; as a consequence, the recirculation downstream of the abutment is no more visible, even if the direct observation of the phenomenon in process showed it was similar to the previous instants. It can be seen anyway that the wake is responsible for the largest sediment fluxes.

The activity regions are similar to those previously described; yet there is no systematic increase of the solid discharge along the streamlines. This would indicate the presence of movements that do not result in real migration of the sediments, but rather in displacements that are not effective for the sediment leaving the hole and thus for the scour depth increase. This is particularly evident for the trapezoidal abutment. For the latter, the action of the principal vortex is now evident from some upward movements near the channel wall. The sediment pattern around the vertical plate is more complicated: there are two zones of relatively considerable activity (near the channel wall for $x \cong 830$ mm and upstream of the abutment nose, $x \cong 940$ mm and $y \cong 120$ mm), where the solid discharge assumes relatively high values and the sediment streamlines are considerably directed upstream. This is particularly evident also for the successive stages of the erosion process, as is shown in Fig. 10. This observation can be interpreted with the existence of two vortical systems, the first of which is larger and localized near the channel wall, while the second is smaller and located upstream of the abutment edge. It is interesting to note that the smaller vortex is reasonably responsible for the formation of the sediment hill in the same position

(compare Figs. 10 and 5, even if they are for different scour levels). The larger vortex is present also upstream of the trapezoidal abutment, while the smaller is typical of the vertical plate, again due to the bluntness of such obstacle.

Figs. 11 and 12 present some spatial distributions of the variation coefficient CV of the solid discharge (CV is defined as the ratio between the standard deviation and the mean value of the solid discharge sample). It can be seen that irregularity of the scour process increases for growing scour depth (and thus for smaller sediment activity), as was found also in previous works ([8] and [10]). Comparison between the maps for the vertical plate and the trapezoidal abutment shows that irregularity of the scour process is larger for the streamlined obstacle, indicating again that there is a correspondence between small activity and large irregularity. The last consideration is enforced by the observation that, for both the experimental times we show, the areas where there are the maximum flux are also those where the coefficient of variation is minimum. This was interpreted admitting that in all the locations the flow field can reach similar maximum intensity, but this leads to high irregularities where the mean intensity is rather weak.

VI. CONCLUSIONS

In this work we analyzed the scour development and the sediment motion around bridge abutments. The experiments were run in a pressurized duct to allow for optimal vision conditions, essential for acquiring films of the sediment motion to be processed to obtain quantitative indicators. We tested two types of abutment, a vertical plate and a trapezoidal obstacle, to investigate similarities and discrepancies in the scour process due to the abutment shape.

The scour depth evolution is consistent with those obtained during experiments with a free surface; dimensionless maximum scour depth at the trapezoidal abutment is about 75 % of that at the vertical plate.

Data on the sediment kinematics were analyzed to infer the description of the scouring flow field. The average solid discharge for certain locations and evolution stages was assumed as an indicator of the sediment activity and of the erosive power of the flow field. The sediment activity decreases for both the obstacles as the process develops.

The sediment patterns at the obstacles are rather similar in the initial phase of the process, where the principal vortex system is highly stretched along the main direction in both cases. Next, bluntness of the vertical plate determines a larger evidence of the three-dimensional vortical systems: the principal vortex is present at both the abutments, even if it is weaker in the trapezoidal case; in the vertical plate, a second vortex system develops upstream of the abutment nose, that is not present in the trapezoidal case. Some features of the scour hole shape were interpreted on the basis of the observations on the sediment motion.

Irregularity of the sediment motion is inversely proportional to sediment activity. Thus, the variation coefficient of the solid discharge increases in time, being much larger in case of the trapezoidal abutment than in that of the vertical plate.

REFERENCES

[1] G. Oliveto and W.H. Hager, "Temporal evolution of clear water pier and abutment scour", *J. Hydraul. Eng.*, vol. 128, pp. 811-820, 2002.

[2] S.E. Coleman, C.S. Lauchlan and B.W. Melville, "Clear-water scour development at bridge abutments", *J. Hydraul. Res.*, vol. 41, pp. 521-531, 2003.

[3] B. Dargahi, "The turbulent flow field around a circular cylinder", *Exp. Fluids*, vol. 8, pp. 1-12, 1989.

[4] R.T.F. Kwan and B.W. Melville, "Local scour and flow measurements at bridge abutments", *J. Hydraul. Res.*, vol 32, pp. 661-673, 1994.

[5] F. Ahmed and N. Rajaratnam, "Observations on flow around bridge abutment", *J. of Engineering Mechanics*, vol. 126, pp- 51-59, 2000.

[6] M.H. Tseng, C.L. Yen and C.C.S. Song, "Computation of three-dimensional flow around square and circular piers", *Int. J. Numer. Meth. Fl.*, vol. 34, pp. 207-227, 2000.

[7] A. Chrisohoides, F. Sotiropulos and T.W. Sturm, "Coherent structures in flat-bed abutment flow: computational fluid dynamics simulations and experiments", *J. Hydraul. Eng.*, vol. 129, pp. 177-186, 2003.

[8] S. Malavasi, A. Radice, and F. Ballio, "Study of Sediment Motion in a Local Scour Hole through an Image Processing Technique", *River Flow 2004, II Int. Conf. on Fluvial Hydraulics, Naples, Italy*, 2004, vol. 1, pp. 535-542, 2004.

[9] A. Radice, S. Malavasi, and F. Ballio, "PIV Analysis of Sediment Kinematics in an Abutment Scour Hole", *ICSE 2004, II Int. Conf. on Scour and Erosion, Singapore*, vol. 2, pp.359-366, 2004.

[10] A. Radice, S. Malavasi, and F. Ballio, "Time Evolution of Erosion Depth and Sediment Motion for Abutment Scour in a Pressure Duct", *River Flow 2006, III Int. Conf. on Fluvial Hydraulics, Lisbon, Portugal*.

[11] A. Radice, S. Franzetti, and F. Ballio, "Prove Sperimentali di Erosione Localizzata in un Condotto Rettangolare in Pressione (Local Scour Experiments in a Rectangular Pressurized Duct)", *XXX Convegno di Idraulica e Costruzioni Idrauliche, Roma* (in italian).

[12] B.W. Melville, "Pier and Abutment Scour: Integrated Approach", *J. Hydraul. Eng.*, vol. 123, pp. 125-136, 1997.

[13] F. Ballio and E. Orsi, "Time evolution of scour around bridge abutments", *Water Engineering Research*, vol. 2, pp. 243-259, 2001.

[14] W. H. Wong, "Scour at bridge abutments", *Report n. 275, University of Auckland, Auckland, New Zealand*, 1982.

[15] R.T.F. Kwan, "A study of abutment scour", *Report n. 451, University of Auckland, Auckland, New Zealand*, 1988.

[16] A. Radice, "Cinematica dei Sedimenti in un Fenomeno Erosivo Localizzato (Sediment Kinematics in a Local Scour Phenomenon)", *PhD Thesis, Politecnico di Milano, Milan, Italy*, 2005 (in italian).

[17] S. Ouillon and D. Dartus, "Three-dimensional computation of flow around groyne", *J. Hydraul. Eng.*, vol. 123, pp. 962-970, 1997.

[18] A. Teruzzi, S. Salon, F. Ballio and V. Armenio, "Numerical investigation of the turbulent flow around a bridge abutment", *River Flow 2006, III Int. Conf. on Fluvial Hydraulics, Lisbon, Portugal*.

[19] V. Armenio, E. Caroni and V. Fiorotto, discussion to "Equilibrium clear-water scour around an abutment", *J. Hydraul. Eng.*, vol. 124, pp. 1069-1070, 1998.

[20] B.W. Melville and A. J. Raudkivi, "Flow characteristics in local scour at bridge piers", *J. Hydraul. Res.*, vol. 15, pp. 373-380, 1977.